DOI: 10.13009/EUCASS2017-664

Magnetic Attitude Control for the MOVE-II Mission

David Messmann[1†], *Felipe Coelho*[2], *Philipp Niermeyer*[1], *Martin Langer*[1], *He Huang*[3], *Ulrich Walter*[1]
[1]*Technical University of Munich*
Boltzmannstrasse 15, 85748 Garching, Germany
[2]*Federal University of Santa Maria, Brazil*
[3]*Northwestern Polytechnical University, China*
david.messmann@tum.de · felipesn.coelho@gmail.com
[†]Corresponding author

Abstract
This paper presents the fundamental work on the attitude control design using solely magnetic actuation for the MOVE-II mission. Two control modes are primarily considered: detumbling and sun pointing control. Regarding the sun pointing control, two approaches are discussed. The first is the Spin Stabilized Sun Pointing Control (SSPC) which provides gyroscopic stiffness against disturbances. The second is a non-spinning approach called Reduced Sun Pointing Control (RSPC). Simulation results have shown satisfactory performance providing proof of concept and motivation for further work.

1. Introduction

MOVE-II (Munich Orbital Verification Experiment II) is a CubeSat currently developed in the Institute of Astronautics (LRT) of the Technical University of Munich (TUM).[1] As a follow-up of the First-MOVE[2,3] mission, which utilized permanent magnets and hysteresis rods for passive attitude stabilization, MOVE-II, shown in Fig. 1, will be the first CubeSat of the LRT with active attitude control. MOVE-II is a 1U CubeSat ($10 \times 10 \times 10\,\mathrm{cm}^3$) comprising six printed circuit boards (PCBs), five of them located on the satellite's outside: the Toppanel and Sidepanels. The Toppanel is similar to the Sidepanels, but it also features the payload solar cells and its electronics. The ADCS mainboard, which is called Mainpanel, is located in the board stack of the satellite. The complete ADCS hardware is depicted in Fig. 2. Linked to the Toppanel, the Flappanels (see Fig. 1), which will be deployed during launch and early operation phase (LEOP), features also solar cells. The Toppanel and the front side of the Flappanels have to be directed towards the sun in order to guarantee power generation, charging of the battery, and also the success of the payload experiments. Attached to the bottom of the satellite is the communication subsystem including an S-band system with a limited transmit and receive angle. Following mission analysis, it turns out that nadir pointing attitude is not suitable to ensure sufficient communication coverage, yet a sun pointing attitude has shown to improve communication with the ground station as well as guarantees power generation for a fully operational satellite.

Regarding the particular case of the sun pointing problem, the paper presents two candidate solutions. The first technique considers spin stabilization in order to exploit the spin axis stiffness against external disturbances. A simple sun pointing control law combined with gyroscopic spin stabilization is proposed in Sedlund[4] as the contingency mode, when only analog-output sensors (three-axis magnetometer and sun sensors), analog-input actuators (magnetic torque rods or coils) and a simple microprocessor are available. More recent research have also presented similar approach and provided further analysis in spin stabilization for solely magnetically actuated satellites.[5–8] In order to achieve passive spin stabilization a rotation around the major or minor axes of inertia of a rigid body is required. However, in real applications satellites cannot be considered as a completely rigid body due to the presence of flexible structures. MOVE-II, for instance, features semi-rigid antennas, which can oscillate in space. This would result in small dissipative effects making the minor axis of inertia unstable. The current determination of the inertia tensor of MOVE-II implies that the axis of interest for sun pointing matches the intermediate axis of inertia of the MOVE-II CubeSat, which results in an unstable motion. Thus, a second technique considers a non-spinning control resolving both stabilization and sun pointing task. A simple but effective controller is designed able to drive the satellite to stability from large rotational rates and to maintain the solar panels facing the sun. Attitude knowledge is not necessarily required for the proposed sun pointing algorithms, as the sun vector can be explicitly used in the state feedback. Both approaches are formulated as a linear quadratic regulation (LQR) problem. Since a complete control synthesis and stability proof is desired, the control design procedure presented in Wisniewski[9] for a three-axis stabilization problem is reused.

DOI: 10.13009/EUCASS2017-664

The paper presents the B-dot control and the sun pointing control approaches. The latter ones are presented in detail. Therefore, controller design and stability analysis are conducted. The concept is investigated through simulations considering external disturbances.

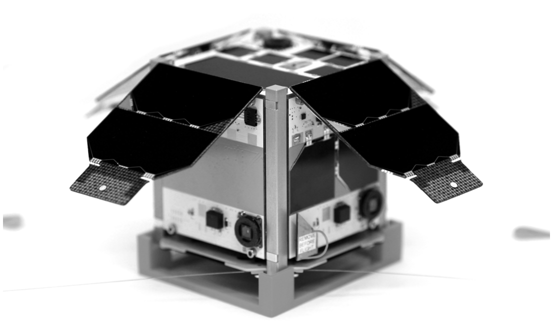

Figure 1: The assembled engineering model of the MOVE-II satellite

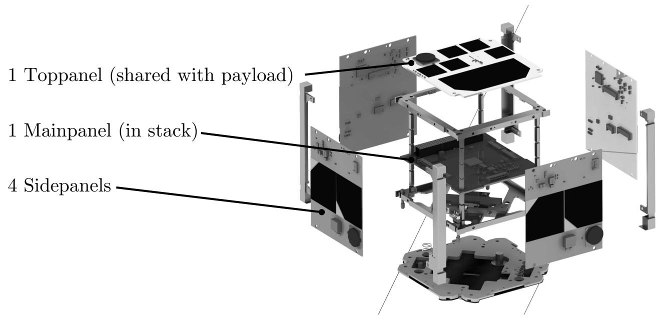

Figure 2: Explosion rendering of the ADCS hardware. The Mainpanel, the Toppanel and one Sidepanel are marked.

2. System Modelling

The satellite's attitude kinematics and rotational dynamics are described hereinafter. The nonlinear equations of motion are used to simulate the satellite, whereas the linearized equations of motion are utilized for the control design. Firstly, we define the two coordinate frames considered through this paper as follows.

2.1 Coordinate Frames

Inertial Frame. The inertial frame is fixed in space placed at the center of the Earth. Denoted by frame $\mathcal{F}_i$, $+z_i$-axis lies along the Earth's axis of rotation, $+x_i$-axis lies along the equator plane pointing towards the *vernal equinox*, and $+y_i$ completes the Cartesian coordinate system.

Body Frame. The body frame is attached to the center of mass of the satellite, aligned with the principal axes of inertia. The body frame is denoted by $\mathcal{F}_b$. Let MOVE-II be approximated by a perfect cube with uniformly homogeneous mass distribution. The z_b-axis is directed away from the Toppanel. Thus, in a sun directed attitude, the sun vector resolved in $\mathcal{F}_b$ is given by $\boldsymbol{s}^b = (0, 0, -1)^T$. At times, subscript b may be omitted when the reference is implicit.

2.2 Equations of Motion

Let the attitude of the satellite with respect to the $\mathcal{F}_i$ be represented by a quaternion $\boldsymbol{q}_{ib} \equiv (q_0, \boldsymbol{\varrho}^T)^T \in \mathbb{R}^4$, where $\boldsymbol{\varrho} = (q_1, q_2, q_3)^T$, and the angular velocity of the body relative to the $\mathcal{F}_i$ expressed in the $\mathcal{F}_b$ be denoted by $\boldsymbol{\omega}_{ib}^b = (\omega_1, \omega_2, \omega_3)^T$. The quaternion-based kinematic equations can be decomposed as follows:

$$\dot{q}_0 = -\frac{1}{2}\boldsymbol{\varrho}^T \boldsymbol{\omega}_{ib}^b \tag{1}$$

$$\dot{\boldsymbol{\varrho}} = \frac{1}{2}\left(q_0 \boldsymbol{I}_{3\times3} + [\boldsymbol{\varrho}\times]\right)\boldsymbol{\omega}_{ib}^b \tag{2}$$

where $[\cdot\times]$ corresponds to the cross-product operator defined as

$$[\boldsymbol{v}\times] \equiv \begin{bmatrix} 0 & -v_3 & v_2 \\ v_3 & 0 & -v_1 \\ -v_2 & v_1 & 0 \end{bmatrix} \tag{3}$$

Now consider the satellite as a rigid body described by the inertia matrix $\boldsymbol{J}$ approximated as

$$\boldsymbol{J} = \begin{bmatrix} J_{11} & 0 & 0 \\ 0 & J_{22} & 0 \\ 0 & 0 & J_{33} \end{bmatrix} \tag{4}$$

DOI: 10.13009/EUCASS2017-664

Then applying the Euler's equation for a rotative body, the dynamic equation of the satellite can be described as

$$\begin{aligned} \dot{\boldsymbol{\omega}}_{ib}^{b} &= \boldsymbol{J}^{-1}\left(\boldsymbol{J}\boldsymbol{\omega}_{ib}^{b} \times \boldsymbol{\omega}_{ib}^{b} + \boldsymbol{\tau}_{ctrl}^{b} + \tau_{d}^{b}\right) \\ &= g\left(\omega_{ib}^{b}, \boldsymbol{\tau}_{ctrl}^{b}, \boldsymbol{\tau}_{d}^{b}\right) \end{aligned} \tag{5}$$

where $\boldsymbol{\tau}_{ctrl}^{b} \in \mathbb{R}^3$ refers to the control torque performed by the satellite and $\boldsymbol{\tau}_{d}^{b} \in \mathbb{R}^3$ refers to disturbance torques acting on the satellite.

2.3 Magnetic Actuation

The MOVE-II satellite is solely magnetically actuated by magnetorquers. The magnetic attitude control problem is intrinsically nonlinear and time-varying as the actuation is based on the interaction between the magnetic dipole momentum generated by a set of three orthogonal current-driven coils and the local geomagnetic field. Consequently, the control design becomes non-trivial yet it has been shown that the attitude stabilization and controllability are achievable for a wide range of orbit inclinations.[10–14] In order to model the magnetic actuation in the dynamic equation of motion, let the control torque be described as

$$\begin{aligned} \boldsymbol{\tau}_{ctrl} &= \boldsymbol{m} \times \boldsymbol{b} \\ &= [\boldsymbol{b}\times]^{T}\, \boldsymbol{m} \end{aligned} \tag{6}$$

where $\boldsymbol{m} \in \mathbb{R}^3$ and $\boldsymbol{b} \in \mathbb{R}^3$ are the magnetic dipole momentum generated by the magnetorquers and the geomagnetic field, respectively, expressed in the $\mathcal{F}_b$. It can be verified in equation (6) that the performed control torque only exists in the plane perpendicular to the local geomagnetic field vector, meaning that only two axes can be controlled at once. Indeed, as $[\boldsymbol{b}\times]$ is structurally singular, full controllability is lost at each time instant. It also turns out that parallel components are ineffective to perform the desired maneuver.[10] For convenience, therefore, we can define a mapping formula in order to obtain $\boldsymbol{u} \rightarrow \boldsymbol{m} \perp \boldsymbol{b}$, where $\boldsymbol{u} \in \mathbb{R}^3$ is the control input vector. This mapping formula can be defined as[15]

$$\boldsymbol{m} = \frac{\boldsymbol{u} \times \boldsymbol{b}}{||\boldsymbol{b}||} \tag{7}$$

Substituting (7) in (6), and rearranging the terms, yields

$$\boldsymbol{\tau}_{ctrl} = \frac{[\boldsymbol{b}\times]^{T}\,[\boldsymbol{b}\times]^{T}}{||\boldsymbol{b}||}\boldsymbol{u} = \boldsymbol{\mathcal{B}}\boldsymbol{u} \tag{8}$$

where the magnetic control matrix $\boldsymbol{\mathcal{B}} \geq \boldsymbol{0} \in \mathbb{R}^{3\times 3}$ is given by

$$\boldsymbol{\mathcal{B}} = \frac{1}{||\boldsymbol{b}||}\begin{bmatrix} -b_2^2 - b_3^2 & b_1 b_2 & b_1 b_3 \\ b_1 b_2 & -b_1^2 - b_3^2 & b_2 b_3 \\ b_1 b_3 & b_2 b_3 & -b_1^2 - b_2^2 \end{bmatrix} \tag{9}$$

Due to the periodic nature of the Earth's magnetic field its components are not constant over time. In our investigations we assume that the time-variability mainly results from the orbital period. We can write $\boldsymbol{\mathcal{B}}(t) = \boldsymbol{\mathcal{B}}(T + t)$, where T is the system period, to emphasize the time dependency. According to Lovera[12] Lemma 1, for sufficiently small angular rates $\boldsymbol{\omega}$, average controllability is guaranteed in the sense of

$$\bar{\boldsymbol{\mathcal{B}}} = \lim_{\tau\to\infty} \frac{1}{\tau}\int_0^{\tau} \boldsymbol{\mathcal{B}}(t)dt > \boldsymbol{0} \tag{10}$$

for all trajectories of the model described in equation (5). Henceforth, result obtained in equation (10) can be considered in the control design.

2.4 Disturbances Modelling

Knowing that the MOVE-II is designed to a low-Earth orbit (LEO) mission with an altitude between 500 km to 600 km, three main disturbance torques are of special concern in the present paper: disturbance torque due to (a) gravity gradient, (b) atmospheric drag, and (c) residual magnetic dipole momentum. Modelling equations are provided in the sequel and will be considered in the simulation to assess the controller performance.

DOI: 10.13009/EUCASS2017-664

2.4.1 Gravity Gradient

Disturbance torques due to the gravity gradient results from the inverse square gravitational force field.[16] As the nature of the gravity gradient is known, an analytic formula can be derived as

$$\boldsymbol{\tau}_{gg} = 3\omega_o^2(\hat{\boldsymbol{r}} \times \boldsymbol{J}\hat{\boldsymbol{r}}) \tag{11}$$

where ω_o is the orbital rate and $\hat{\boldsymbol{r}} \in \mathbb{R}^3$ as the normalized position vector. It can be noted that equation (11) depends only on the symmetry of the satellite, i.e. the satellite's moment of inertia, and the current position. Thus, the torque due to gravity gradient should affect just a little considering that the MOVE-II satellite is significantly symmetric.

2.4.2 Atmospheric Drag

The drag force acting on an infinitesimal surface element can be calculated with:[16,17]

$$d\boldsymbol{F} = -\frac{1}{2}C_D\rho v^2\frac{\boldsymbol{v}}{v}(\hat{\boldsymbol{v}} \cdot \boldsymbol{n})dA \tag{12}$$

where ρ is the atmospheric density, $v = ||\boldsymbol{v}||$ is the satellite's velocity relative to the flow, C_D is the drag coefficient and dA is the infinitesimal area, which is normal to the relative velocity $\boldsymbol{v} \in \mathbb{R}^3$. The normal vector is denoted by $\boldsymbol{n} \in \mathbb{R}^3$. Let α be the angle between $\boldsymbol{v}$ and $\boldsymbol{n}$. According to Hughes,[17] the torque should only be calculated according to equation (12) if $\cos\alpha \geq 0$, otherwise dA is not affected by the flow. Therefore, the so-called *Heaviside Function* $\Theta(x)$ has to be introduced, which is $\Theta = 1$ for $x \geq 0$ and $\Theta = 0$ otherwise. Thus, we get

$$d\boldsymbol{F} = -\frac{1}{2}C_D\rho v^2\Theta(\hat{\boldsymbol{v}} \cdot \boldsymbol{n})\hat{\boldsymbol{v}}(\hat{\boldsymbol{v}} \cdot \boldsymbol{n})dA \tag{13}$$

When dA is known, the total force can be calculated by integrating (13). A common approach to solve this integral is to decompose the total spacecraft surface into elementary shapes, e.g. planes . The drag force $\boldsymbol{F}_i \in \mathbb{R}^3$ can be calculated simply for each plane A_i by

$$\boldsymbol{F}_i = -\frac{1}{2}C_D\rho v^2\Theta(\hat{\boldsymbol{v}} \cdot \boldsymbol{n}_i)\hat{\boldsymbol{v}}(\hat{\boldsymbol{v}} \cdot \boldsymbol{n}_i)A_i \tag{14}$$

The corresponding drag torque acting on this surface is given by

$$\boldsymbol{\tau}_i = \boldsymbol{F}_i \times \boldsymbol{l}_i \tag{15}$$

with $\boldsymbol{l}_i \in \mathbb{R}^3$ as the distance vector from the center of mass and the center of pressure of the surface A_i. The total atmospheric drag toque is the vector sum of the individual torques:

$$\boldsymbol{\tau}_D = \sum_i \boldsymbol{\tau}_i \tag{16}$$

As depicted in Fig.3, the MOVE-II satellite can be approximated by planes, but due to the configuration of the Flap-panels overshadowing effect occurs blocking the incident flow denoted by v_{rel} against the Sidepanels, and vice-versa. An analytic expression to describe such a configuration is rather beyond of the scope of this paper and, therefore, an approximated expression is considered. Another important aspect is the appropriate modelling of the atmospheric density ρ. In our simulation the density has been calculated by the *MSIS-E-90 Atmosphere Model* provided by NASA.[18]

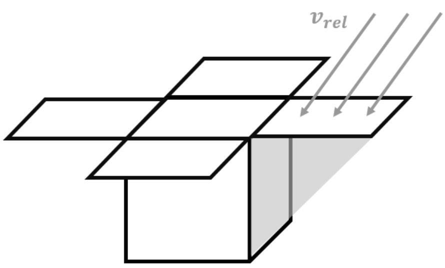

Figure 3: Overshadowing effect of the panels

DOI: 10.13009/EUCASS2017-664

2.4.3 Residual Magnetic Dipole Moment

In practice, when all subsystems operate as a whole, undesired magnetic dipole moments may be built up by on-board electronics, scientific instruments and ferromagnetic materials resulting in a residual dipole momentum $\boldsymbol{m}_{RMM}$, i.e., a magnetic bias, that can disturb the stability and maneuverability of the satellite. As an example, the UWE-3 mission encountered an estimated residual dipole moment of $\boldsymbol{m}_{RMM} \approx (-0.001, 0.012, -0.045) \pm 0.001Am^2$ that affected the motion of the satellite.[19] Recalling equation (6), therefore, the disturbance torque due to residual magnetic dipole momentum, $\boldsymbol{\tau}_{RMM}$, can be modelled as

$$\boldsymbol{\tau}_{RMM} = \boldsymbol{m}_{RMM} \times \boldsymbol{b} \tag{17}$$

For our investigations we assume that the residual magnetic dipole moment is a constant offset.

2.5 Linearized Model

As aforementioned, attitude knowledge is not necessarily required in the formulation of the sun pointing problem. Instead, it is of the interest to replace the quaternion-based kinematic equation (2) with an adapted model as function a of the sun vector $\boldsymbol{s}^b \in \mathbb{R}^3$ seen from the $\mathcal{F}_b$ as follows:

$$\begin{aligned} \dot{\boldsymbol{s}}^b &= -\boldsymbol{\omega}_{ib}^b \times \boldsymbol{s}^b \\ &= f(\boldsymbol{s}^b, \boldsymbol{\omega}_{ib}^b) \end{aligned} \tag{18}$$

Considering the sun vector-based kinematic equation (18) and recalling the dynamics in (5), the satellite model can be described in the state-space form linearizing the system about a desired equilibrium state. Then, let the equilibrium state be $\bar{\boldsymbol{s}}^b = (0, 0, -1)^T$ and $\bar{\boldsymbol{\omega}}_{ib}^b = (0, 0, \omega_S)^T$, where ω_S refers to spin rate about the z-axis of the body frame, yielding the linear system

$$\begin{aligned} \delta\dot{\boldsymbol{x}} &= \begin{bmatrix} \dfrac{\partial f(\bar{\boldsymbol{s}}^b, \bar{\boldsymbol{\omega}}_{ib}^b)}{\partial \boldsymbol{s}^b} & \dfrac{\partial f(\bar{\boldsymbol{s}}^b, \bar{\boldsymbol{\omega}}_{ib}^b)}{\partial \boldsymbol{\omega}_{ib}^b} \\ \dfrac{\partial g\left(\bar{\boldsymbol{\omega}}_{ib}^b, \boldsymbol{\tau}_{ctrl}^b\right)}{\partial \boldsymbol{s}^b} & \dfrac{\partial g\left(\bar{\boldsymbol{\omega}}_{ib}^b, \boldsymbol{\tau}_{ctrl}^b\right)}{\partial \boldsymbol{\omega}_{ib}^b} \end{bmatrix} \delta\boldsymbol{x} + \begin{bmatrix} \dfrac{\partial f(\bar{\boldsymbol{s}}^b, \bar{\boldsymbol{\omega}}_{ib}^b)}{\partial \boldsymbol{u}^b} \\ \dfrac{\partial g\left(\bar{\boldsymbol{\omega}}_{ib}^b, \boldsymbol{\tau}_{ctrl}^b\right)}{\partial \boldsymbol{u}^b} \end{bmatrix} \boldsymbol{u} \\ &= \boldsymbol{A}\delta\boldsymbol{x} + \boldsymbol{B}\boldsymbol{u} \end{aligned} \tag{19}$$

Solving the Jacobian equations in (19), the state matrix $\boldsymbol{A}$ and the control input matrix $\boldsymbol{B}$ are, therefore, given by

$$\boldsymbol{A} = \begin{bmatrix} 0 & \omega_S & 0 & 0 & 1 & 0 \\ -\omega_S & 0 & 0 & -1 & 0 & 0 \\ 0 & 0 & 0 & 0 & 0 & 0 \\ 0 & 0 & 0 & 0 & \omega_S\sigma_1 & 0 \\ 0 & 0 & 0 & -\omega_S\sigma_2 & 0 & 0 \\ 0 & 0 & 0 & 0 & 0 & 0 \end{bmatrix}, \quad \boldsymbol{B}(t) = \begin{bmatrix} \boldsymbol{0}_{3\times3} \\ \boldsymbol{J}^{-1}\mathcal{B}(t) \end{bmatrix} \tag{20}$$

$$\sigma_1 = \frac{J_{22} - J_{33}}{J_{11}}, \quad \sigma_2 = \frac{J_{11} - J_{33}}{J_{22}}$$

The model represents a time-periodic system, since $\boldsymbol{B}(t) = \boldsymbol{B}(T + t)$. Moreover, the system described in equations (19)-(20) can be rather reduced. In fact, it can be verified that matrix $\boldsymbol{A}$ has the third row and the third column with zeroed elements, allowing us to define the system into a reduced form given by

$$\delta\dot{\boldsymbol{x}}_r = \boldsymbol{A}_r\delta\boldsymbol{x}_r + \boldsymbol{B}_r(t)\boldsymbol{u} \tag{21}$$

$$\delta\boldsymbol{x}_r = \begin{bmatrix} s_1 \\ s_2 \\ \omega_1 \\ \omega_2 \\ \omega_3 - \omega_S \end{bmatrix}, \quad \boldsymbol{A}_r = \begin{bmatrix} 0 & \omega_S & 0 & 1 & 0 \\ -\omega_S & 0 & -1 & 0 & 0 \\ 0 & 0 & 0 & \omega_S\sigma_1 & 0 \\ 0 & 0 & -\omega_S\sigma_2 & 0 & 0 \\ 0 & 0 & 0 & 0 & 0 \end{bmatrix}, \quad \boldsymbol{B}_r(t) = \begin{bmatrix} \boldsymbol{0}_{2\times3} \\ \mathcal{B}(t) \end{bmatrix} \tag{22}$$

When equation (10) is used to calculate an average control input matrix, the reduced linear system (21)-(22) is fully controllable and, therefore, can be used to find a static gain controller.

DOI: 10.13009/EUCASS2017-664

3. Control Design

Control laws are introduced for two mission phases specified earlier: (a) detumbling and (b) sun pointing mode. The first mode concerns the imminent scenario encountered by the satellite after its deployment. Special attention is given to the latter mode for two different control approaches. Therefore, model-based state-feedback control approach is utilized. For a first guess, an LQR formulation is used to design a controller gain. Afterwards the stability of the closed-loop system is analyzed with the Floquet theory for time-periodic systems.[20]

3.1 Detumbling Control

Right after deployed, satellites are likely to experience angular rates higher than usually desired. The so-called B-dot algorithm is a simple and commonly applied method for detumbling a satellite. This method does not require attitude knowledge, but rather only the rate of change of the local geomagnetic field as follows:

$$\boldsymbol{m}^b = -k\dot{\boldsymbol{b}}^b \tag{23}$$

where $\boldsymbol{m}^b$ is the control dipole moment, k is a positive scalar gain and $\dot{\boldsymbol{b}}^b$ is expressed with respect to $\mathcal{F}_b$. Assuming that the rate of change of the geomagnetic field is negligible compared to the attitude rate,[9] the formula (23) can be approximated by

$$\begin{aligned} \boldsymbol{m}^b &= -k\left(\boldsymbol{b}^b \times \boldsymbol{\omega}^b_{ib} + \boldsymbol{A}(\boldsymbol{q}^{bi})\dot{\boldsymbol{b}}^i\right) \\ &\approx -k\left(\boldsymbol{b}^b \times \boldsymbol{\omega}^b_{ib}\right) \end{aligned} \tag{24}$$

with $\boldsymbol{A}(\boldsymbol{q}^{bi})$ as the attitude matrix which corresponds to $\boldsymbol{q}^{bi}$. We refer to Jensen[21] for the stability proof of the B-dot control.

3.2 Sun Pointing Control

Considering the reduced system obtained in (21), two constant gain sun pointing controllers can be obtained relying in the solution of the LQR problem as shown in the sequel. For simplification, we define $\boldsymbol{x} \equiv \delta\boldsymbol{x}_r$, $\boldsymbol{A} \equiv \boldsymbol{A}_r$ and $\boldsymbol{B} \equiv \boldsymbol{B}_r$.

3.2.1 Control Synthesis

Based on the optimal control theory, the LQR problem solves the optimal state feedback law $\boldsymbol{u} = -\boldsymbol{K}\boldsymbol{x}$ by minimizing a performance index

$$\mathcal{J} = \frac{1}{2}\int\left(\boldsymbol{x}^T\boldsymbol{Q}\boldsymbol{x} + \boldsymbol{u}^T\boldsymbol{R}\boldsymbol{u}\right)dt \tag{25}$$

where $\boldsymbol{Q} \geq \boldsymbol{0}$ and $\boldsymbol{R} > \boldsymbol{0}$ are design matrices with appropriate dimensions which relate the state transient energy and the control input energy, respectively. Then the constant gain matrix $\boldsymbol{K} \in \mathbb{R}^{3\times5}$ can be derived from the steady-state solution as

$$\boldsymbol{K} = \boldsymbol{R}^{-1}\bar{\boldsymbol{B}}^T\boldsymbol{P} \tag{26}$$

where $\bar{\boldsymbol{B}}$ is the averaged control input matrix and $\boldsymbol{P}$ is the unique positive definite solution to the algebric Riccati equation:

$$\boldsymbol{P}\boldsymbol{A} + \boldsymbol{A}^T\boldsymbol{P} - \boldsymbol{P}\bar{\boldsymbol{B}}\boldsymbol{R}^{-1}\bar{\boldsymbol{B}}^T\boldsymbol{P} + \boldsymbol{Q} = \boldsymbol{0} \tag{27}$$

The control input matrix is averaged over one system period T.

3.2.2 Stability Analysis

After calculation of the gain, stability of the closed-loop system has to be analyzed. According to Wisniewski[9] this check is necessary, since stability of the time-varying system is not equivalent with the corresponding time-invariant model. The closed-loop system to be analyzed is given by

$$\dot{\boldsymbol{x}} = \boldsymbol{A}_c(t)\boldsymbol{x} = (\boldsymbol{A} - \boldsymbol{B}(t)\boldsymbol{K})\boldsymbol{x} \tag{28}$$

where $\boldsymbol{A}_c(t)$ is the corresponding system matrix of closed-loop system. This matrix is time periodic, thus $\boldsymbol{A}_c(t) = \boldsymbol{A}_c(T + t)$. The Floquet theory can be used to investigate stability of this time-periodic system. Therefore, the so-called

DOI: 10.13009/EUCASS2017-664

monodromy matrix $\boldsymbol{\Psi}_{A_c} \in \mathbb{R}^{5\times5}$ has to be introduced. It is the transition matrix at time τ relating the value state vector at time τ to the value after one period $\tau + T$:

$$\boldsymbol{x}(\tau + T) = \boldsymbol{\Psi}_{A_c}(\tau)\boldsymbol{x}(\tau) \tag{29}$$

The characteristic multipliers are the eigenvalues of the monodromy matrix $\boldsymbol{\Psi}_{A_c}(\tau)$. The monodromy matrix is an essential tool for analyzing stability of periodic systems. A periodic system (in continuous or discrete time) is stable if only if its characteristic multipliers belong to the open unit disk in the complex plane.[22] For all computed gains the monodromy matrix is calculated and its characteristic multipliers are analyzed to prove stability.

3.2.3 Spin Stabilized Sun Pointing Control - *SSPC*

The first sun pointing approach proposed is a spin stabilized control method. We use the terminology *Spin Stabilized Sun Pointing Control (SSPC)*. Therefore, $\omega_S \neq 0$ has to be inserted in the reduced linear system (21)-(22). For proof of concept, a first gain is calculated with a desired spin rate of approximately 10 times the orbit period, given by $\omega_S = 0.011\,\text{rads}^{-1}$. The results are given in subsection 4.1. To achieve a stiffer spin axis when disturbance torques are considered, a final gain is computed with a spin rate of approximately 100 times the orbit period, given by $\omega_S = 0.11\,\text{rads}^{-1}$. The results are presented in subsection 4.2. This final gains for *SSPC* is given by matrix $\boldsymbol{K}_{SSPC}$ in (30):

$$\boldsymbol{K}_{SSPC} = \begin{bmatrix} -0.0454 & 0.0677 & -27.3049 & -0.6948 & 0.0000 \\ -0.0794 & -0.0386 & -0.9586 & -27.2337 & 0.0000 \\ 0.0000 & 0.0000 & 0.0000 & 0.0000 & -26.8701 \end{bmatrix} \tag{30}$$

The *SSPC* is expected to decrease the pointing error and also provide spin stiffness against the disturbance effects. After acquiring the desired spin rate, magnetorquers can be shut down for saving power consumption and stabilization is sustained passively only by the gyroscopic effect.

3.2.4 Reduced Sun Pointing Control - *RSPC*

The second controller is referred to as *Reduced Sun Pointing Control (RSPC)*. The *RSPC* is not spin stabilized, thus the controller dampens angular rates of the three axes. Hence, using $\bar{\omega}_s = 0$ for the reduced linear system (21)-(22), a first gain for *RSPC* is calculated according to the proposed control design. The results can be found in subsection 4.1. The gain is refined to yield better performance for disturbance rejection. Stability is analyzed afterwards. The results are presented in subsection 4.2. The refined matrix $\boldsymbol{K}_{RSPC}$ is given by

$$\boldsymbol{K}_{RSPC} = \begin{bmatrix} 0.0000 & 0.7606 & -92.7963 & 0.0000 & 0.0000 \\ -0.7606 & 0.0000 & 0.0000 & -74.7403 & -0.0335 \\ 0.0067 & 0.0000 & 0.0000 & 0.0590 & -0.3803 \end{bmatrix} \tag{31}$$

4. Results

For the upcoming simulation results, the mission orbit is calculated employing the Simplified General Perturbation 4 (SGP4) orbit propagator, which takes orbital perturbations into account. The initial conditions of the classical orbital elements are given in Tab. 1. In addition, the International Geomagnetic Reference Field (IGRF) model is used for simulating the Earth's magnetic field.[23]

The satellite is simulated as a nonlinear plant described by the equations of motion (1)-(5), and disturbance torques are considered in order to assess the performance. For all control law investigations the ideal full state feedback is used, i.e. attitude estimation and sensor measurement models are not considered. Actuator constraints are not implemented as well. The inertia tensor considered for MOVE-II is provided in Tab. 2 and the initial conditions used in the simulations are provided in Tab. 3.

4.1 Proof of Concept

Before disturbance torques are considered, the functionality of SSPC and RSPC are analyzed. For the SSPC approach the passive spin stabilization is considered as well. After reaching the desired spin rate, the magnetic actuation is shut down. Thus, only the stiffness of the spin axis provides the stabilization of the satellite.

In a first simulation the initial conditions given in Tab. 3 are considered. Moreover, no perturbation torques are taken into account. Fig. 4 illustrates the result of the SSPC for a time period of 5 orbits. The SSPC approach

DOI: 10.13009/EUCASS2017-664

Table 1: Orbital Parameter Settings

Parameter	Symbol	Value
Eccentricity	e	0.00001
Semi-major axis	a	6953.1 km
RAAN	Ω	78.12°
Inclination	i	97.63°
Arg.og Perigee	ω	0°
Orbit Epoch	-	17 Jan 2017

Table 2: Inertia Tensor for MOVE-II

Symbol	Value
J_{11}	$0.002\,97\,\mathrm{kgm}^2$
J_{22}	$0.003\,30\,\mathrm{kgm}^2$
J_{33}	$0.003\,20\,\mathrm{kgm}^2$

Table 3: Initial Conditions

Symbol	Value
$\boldsymbol{\omega}_{bi}^{b}$	$\begin{bmatrix} 0.01 & 0.01 & 0.01 \end{bmatrix}$ rad/s
$\boldsymbol{q}_{bi}$	$\begin{bmatrix} 0.9515 & 0.2393 & 0.1893 & 0.0381 \end{bmatrix}$

leads to the desired direction of the satellite. The pointing error converges to zero within the considered time period. Furthermore, the satellite is rotating with the desired spin rate of $\omega_S = 0.011\,\mathrm{rads}^{-1}$. Other spin rates could be applied on the controller successfully. This is not shown in this paper.

Fig. 5 shows the result for RSPC with a first design of the controller gain. The upper plot illustrates how the pointing error decreases over time. Furthermore, the angular velocities converges to zero within the considered time period. Thus, the satellite is pointing to the sun, but does not spin. Since the attitude around this axis is not controlled, it can be arbitrary.

In further simulations, passive spin stabilization is investigated. Therefore, one simulation was run with the inertia tensor given in Tab. 2. After 2.5 orbits the magnetorquers are shut down. Thus, closed-loop control is not active. Without the presence of any torques, the satellite motion behaves in accordance with the description in section 1. The satellite is spinning around the z_b-axis, the intermediate axis of inertia. Thus, the motion becomes unstable. In a second simulation the moments of inertia J_{22} and J_{33} from Tab. 2 are exchanged so that the spin axis is the major principal axis. Again the magnetorquers are shut down after 1.5 orbits. The motion is stable as expected. Thus, passive spin stabilization is possible. The magnetorquers can be switched off if passive spin stabilization is desired. Power consumption can be reduced by using the advantage of a stable spin axis. This requires a rotation around the major axis of inertia which, however, does not match the axis of interest for sun-pointing control. In the case of only active spin stabilization a rotation around the intermediate axis of inertia shall be avoided, since ADCS can be shut down during mission.

4.2 Disturbance Rejection

This subsection presents the performance of the control approaches under disturbance torques. The pointing error caused by the perturbation torques is analyzed. Actuator constraints, sensor artifacts and attitude estimation are not taken into account.

Two simulations are run to determine the pointing error for a spin stabilized satellite. The initial conditions are given in Tab. 3. The original inertia tensor given in Tab. 2 is used. Gravity gradient torque and atmospheric drag torque are considered. The drag torque is modelled by considering Flappanels and a density of $\rho = 2.64 \times 10^{-13}\,\mathrm{kgm}^3$. The panel area is approximated by $0.01\,\mathrm{m}^2$ and the aerodynamic coefficient is set to 2.5. Moreover, a worst-case estimation of the residual dipole moment $\|\boldsymbol{m}_{RMM}\| \approx 20\,\mathrm{mAm}^2$ is considered. A constant offset vector is assumed for simplification:

$$\boldsymbol{m}_{RMM} = \begin{bmatrix} 11.547\,\mathrm{mAm}^2 & 11.547\,\mathrm{mAm}^2 & 11.547\,\mathrm{mAm}^2 \end{bmatrix}^T \tag{32}$$

The following two simulation settings are considered:

DOI: 10.13009/EUCASS2017-664

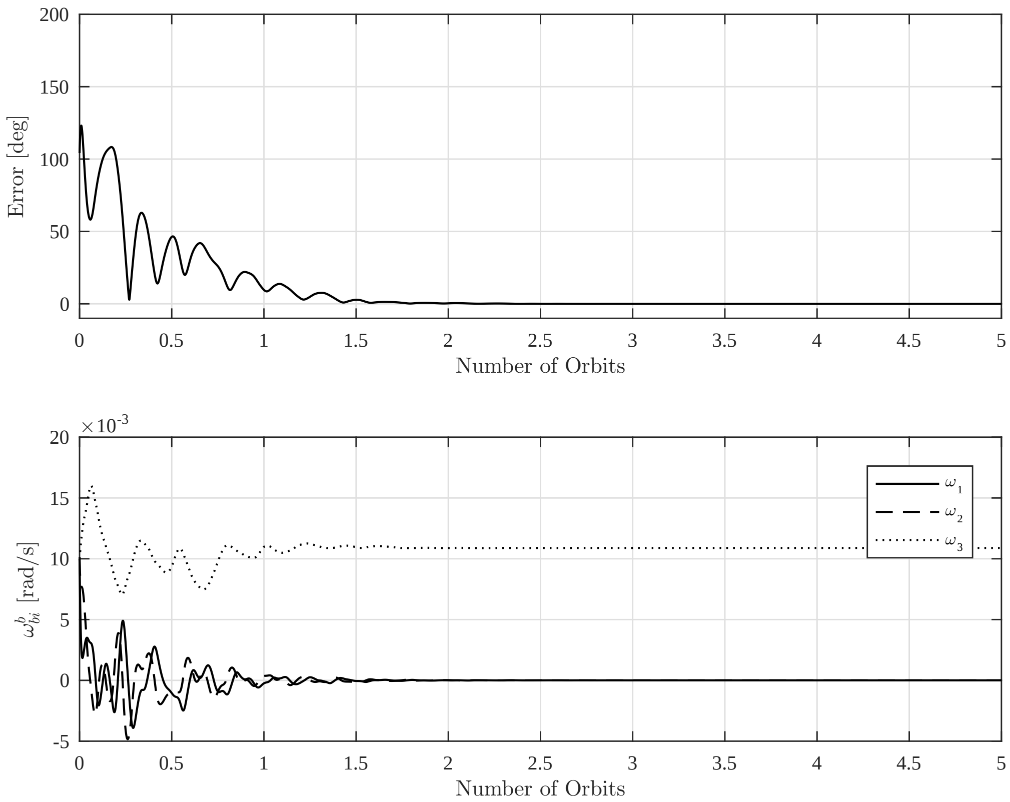

Figure 4: Sun directed spin stabilization: pointing error (top) and angular velocities (bottom)

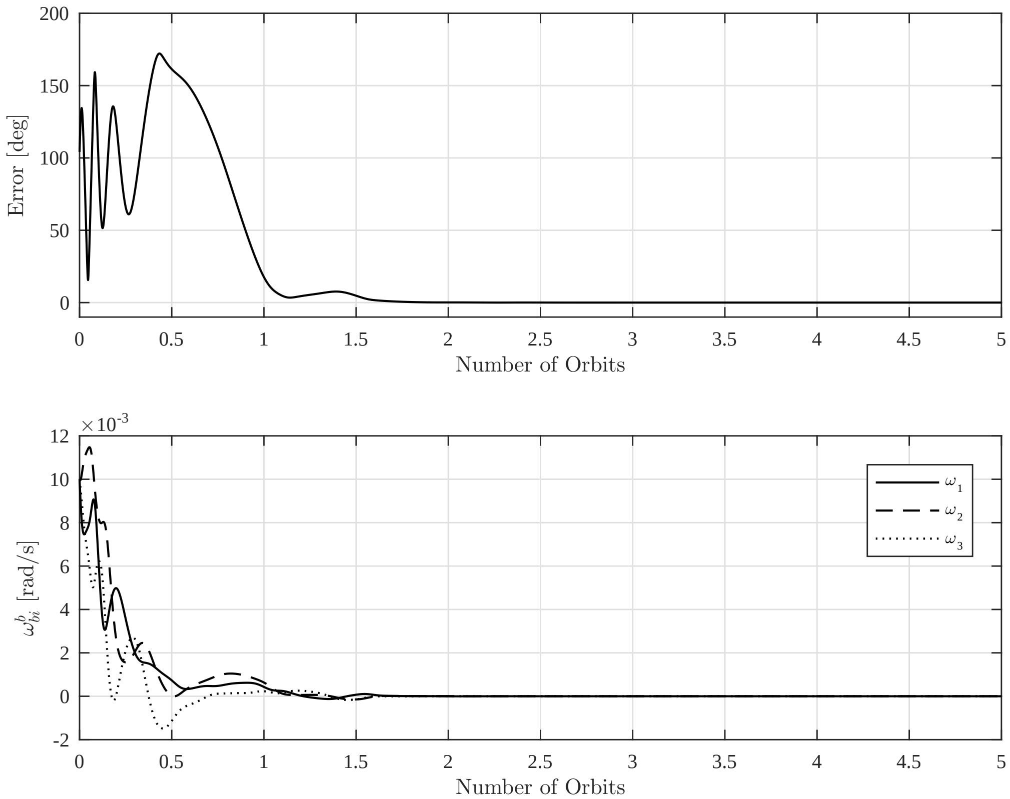

Figure 5: Reduced Sun pointing: pointing error (top) and angular velocities (bottom)

DOI: 10.13009/EUCASS2017-664

A. Spin Stabilization with $\omega_0 = 0.011\,\mathrm{rads}^{-1}$, without residual magnetic dipole moment

B. Spin Stabilization with $\omega_0 = 0.11\,\mathrm{rads}^{-1}$, with residual magnetic dipole moment

In case A no residual dipole moment is considered to assess the impact of only drag and gravitational torque. The result is given in Fig. 6. The error varies over time, having its maximum around 20°. The result shows that spin stabilization is an appropriate technique for disturbance rejection. For better results the spin controller is designed with $\omega_0 = 0.11\,\mathrm{rads}^{-1}$. The gain was introduced in (30). The result for the case B can be seen in Fig. 6. The maximum

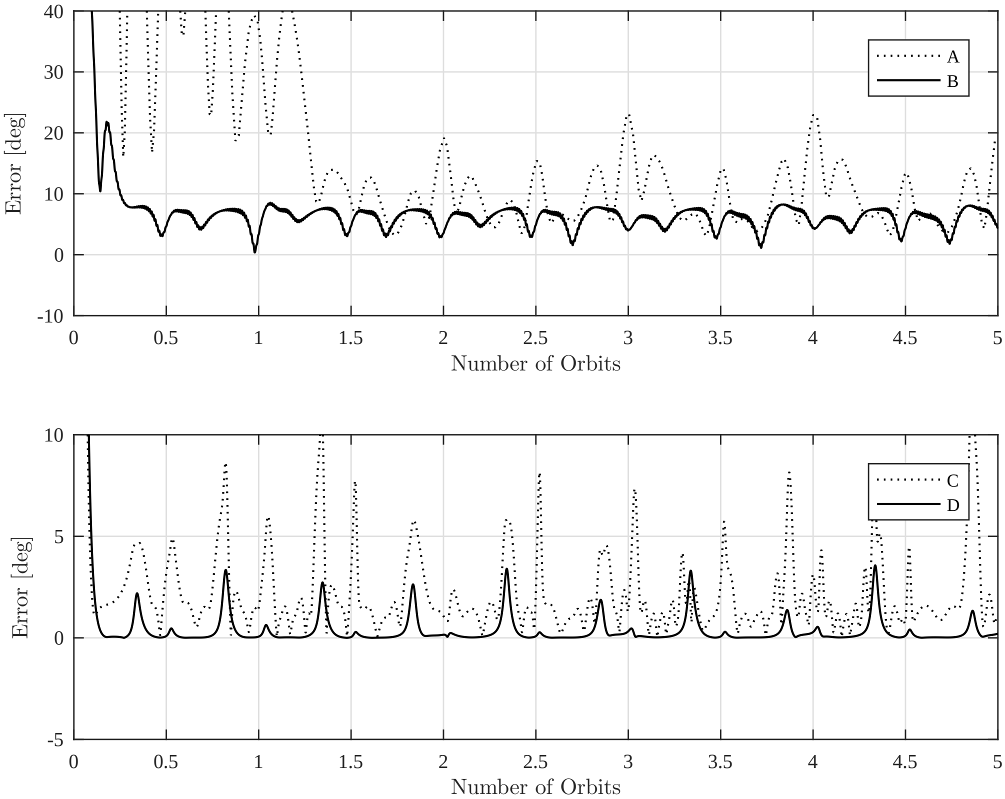

Figure 6: Sun directed spin stabilization: pointing error (top) and angular velocities (bottom)

deviation is below 10°. Thus, a higher spin rate could increase the pointing accuracy. The system in case B could be stabilized. The main idea is to gain a spin axis which is stiff enough to withstand perturbation torques. Depending on the magnitudes of those torques passive spin stabilization also a possible solution. Therefore, an appropriate spin rate has to be chosen.

Two further simulations are run to investigate the performance of the RSPC approach. All parameter settings from the previous testcases are used. The simulations are specified below:

C. $\boldsymbol{K}_{RSPC}$, with residual magnetic dipole moment

D. $\boldsymbol{K}_{RSPC}$, without residual magnetic dipole moment

For both testcases the refined controller gain given in (31) is implemented. In the first simulation (case C) reveals the performance if only drag and gravitational torques are considered. As seen in Fig. 6, the pointing error can be decreased enormously. Maximum deviation is given by 3°. The increased gain entries make the controller more aggressive. Similar performance is observed when the residual dipole moment is considered. The controller is able to suppress the influence of the total disturbance torque. For RSPC, maximum deviation is around 10° and 20° degrees. However, the refined gain leads to a deteriorated performance to stabilize the angular velocity around the pointing axis. However, in both cases the third component of the angular velocity does not converge towards zero. It rather oscillates with an amplitude of around $0.002\,\mathrm{rads}^{-1}$ in case C and $0.02\,\mathrm{rads}^{-1}$ in case D. This behavior is observed, whenever perturbation torques are considered. Nevertheless, the attitude around the pointing axis is not relevant. The rotation around this axis is constrained, no spinning up is observed. Due to those facts and the possibility to increase the pointing accuracy, we accept this limitation.

DOI: 10.13009/EUCASS2017-664

5. Conclusion and Outlook

This paper presented fundamental work on the the attitude control design using only magnetic actuation for the MOVE-II mission. The B-dot control law is introduced as the chosen detumbling controller. Reduced attitude control strategies were investigated as a main objective of this paper instead of control techniques which requires full attitude information. Two main approaches were considered: Spin Stabilized Sun Pointing Control (SSPC) and Reduced Sun Pointing Control (RSPC). Both approaches are sufficient techniques to orient the satellite to the sun. The proof of concept and performance under perturbation torques were shown for both methods.

Both approaches lead to satisfying results. The pointing error could be decreased enormously and the pointing requirement is fulfilled. Since the inertia tensor is not completely determined yet, the risk of unstable spin stabilization exists. If spin stabilization is considered, it is highly recommended to utilize the major axis of inertia for spin axis. Therefore, the RSPC was selected as an appropriate technique for the mission.

Further investigations and tuning procedures of all controllers are undergoing. In the simulation sensor and actuator models will be integrated to assess the performance in more realistic applications. The attitude estimation algorithm will be integrated in order to provide valid data of the complete functionality of the ADCS algorithms. Furthermore, it is considered to adjust the inertia tensor of the satellite so that spin stabilization could be enabled. A Hardware-in-the-Loop (HiL) setup will be developed to test the complete interaction of algorithms implemented in the flight software. Thus, sufficient testing can be guaranteed before launch early 2018.

6. Acknowledgments

The authors acknowledge the funding of MOVE-II by the Federal Ministry of Economics and Energy, following a decision of the German Bundestag, via the German Aerospace Center (DLR) with funding grant number 50 RM 1509.

References

[1] M. Langer, N. Appel, M. Dziura, C. Fuchs, P. Günzel, J. Gutsmiedl, M. Losekamm, D. Meßmann, T. Pöschl, and C. Trinitis. MOVE-II–Der zweite Kleinsatellit der Technischen Universität München. *Deutscher Luft-und Raumfahrtkongress (DLRK) Rostock, Germany*, 2015.

[2] M. Czech, A. Fleischner, and U. Walter. A First-MOVE in Satellite Development at the TU-München. *Small Satellite Missions for Earth Observation*, pages 235–245, 2010.

[3] M. Langer, C. Olthoff, J. Harder, C. Fuchs, M. Dziura, A. Hoehn, and U. Walter. Results and lessons learned from the Cubesat mission First-MOVE. *Small Satellite Missions for Earth Observation, Springer, Berlin*, 2015.

[4] C. Sedlund. A simple sun-pointing magnetic controller for satellites in equatorial orbits. In *IEEE Aerospace Conference*, Big Sky, Montana, 2009.

[5] P. Testani. Development of sun-pointing magnetic attitude control system for CXBN cubesat. In *63rd International Astronautical Congress*, Naples, Italy, 2012.

[6] J. Reijneveld and D. Choukroun. Attitude control system of the Delfi-n3xt satellite. volume 6, pages 189–208, 2013.

[7] M. Y. Ovchinnikov, D. S. Roldugin, and P. Testani. Spin-stabilized satellite with sun-pointing active magnetic attitude control system. *Keldysh Institute Preprints*, 4:p31, 2012.

[8] D. S. Roldugin and P. Testani. Spin-stabilized satellite magnetic attitude control scheme without initial detumbling. *Acta AStronautica*, 94(1):446–454, 2014.

[9] R. Wisniewski. *Satellite Attitude Control Using Only Electromagnetic Actuation*. PhD thesis, Department of Control Engineering, Aalborg University, Aalborg, Denmark, December 1996.

[10] R. Wisniewski. Linear time varying approach to satellite attitude control using only electromagnetic actuation. *Journal of Guidance, Control and Dynamics*, 23(4):640–647, 2000.

[11] M. Lovera, E. de Marchi, and S. Bittanti. Periodic attitude control techniques for small satellites with magnetic actuators. *IEEE Transactions on Control and Systems Technology*, 10(1):90–95, 2002.

DOI: 10.13009/EUCASS2017-664

[12] M. Lovera and A. Astolfi. Spacecraft attitude control using magnetic actuators. *Automatica*, 40(8):1405–1414, 2004.

[13] E. Silani and M. Lovera. Magnetic spacecraft attitude control: a survey and some new results. *Control Engineering Practice*, 13(3):357–371, 2005.

[14] Y. Yang. Controllability of spacecraft using only magnetic torques. *IEEE Transactions on Aerospace and Electronic Systems*, 52(2):954–961, 2016.

[15] R. Wisniewski and M. Blanke. Fully magnetic attitude control for spacecraft subject to gravity gradient. *Automatica*, 35(7):1201–1214, 1999.

[16] J. R. Wertz. *Spacecraft Attitude Determination and Control*. Kluwer Academic Publishers, 1978.

[17] P.C. Hughes. *Spacecraft Attitude Dynamics*. Dover Books on Aeronautical Engineering. Dover Publications, 2012.

[18] N. Papitashvili. *Virtual Ionosphere, Thermosphere, Mesosphere Observatory (VITMO) MSIS-E-90 Atmosphere Model*. https://cohoweb.gsfc.nasa.gov/vitmo/msis_vitmo.html.

[19] S. Busch, P. Bangert, S. Dombrovski, and K. Schilling. UWE-3, in-orbit performance and lessons learned of a modular and flexible satellite bus for future pico-satellite formations. *Acta Astronautica*, 117:73–89, 2015.

[20] R. Wisniewski. Nonlinear control for satellite detumbling based on magnetic torquing. page 10A, Arizona, 1994.

[21] K. Jensen and K. Vinter. *Attitude Determination and Control System for AAUSAT3*. Master thesis, Aalborg University, 2010.

[22] S. Bittanti and P. Colaneri. *Periodic Systems: Filtering and Control*. Communications and Control Engineering. Springer, 2009.

[23] IAGA. International Geomagnetic Reference Field. `https://www.ngdc.noaa.gov/IAGA/vmod/igrf.html`.